Chinese Chemical Letters 37 (2026) 111849

Contents lists available at ScienceDirect

Chinese Chemical Letters

journal homepage: www.elsevier.com/locate/cclet

Significantly improving the performances of thermal conductivity and thermal expansion in aluminum matrix composites through a multiphase design strategy

Jinrui Qian[a], Yue Sun[a], Feixiang Long[a], Yiqing Liu[a], Guozhen Chang[a], Yuzhu Song[a], Naike Shi[a], Andrea Sanson[c], Xiuzhu Han[a,*], Chang Zhou[a,b,*], Jun Chen[a]

[a] Beijing Advanced Innovation Center for Materials Genome Engineering, Department of Physical Chemistry, University of Science and Technology Beijing, Beijing 100083, China
[b] State Key Laboratory for Advanced Metals and Materials, University of Science and Technology Beijing, Beijing 100083, China
[c] Department of Physics and Astronomy, University of Padova, Padova I-35131, Italy

ARTICLE INFO

Article history:
Received 11 July 2025
Revised 8 September 2025
Accepted 17 September 2025
Available online 17 September 2025

Keywords:
Metal matrix composites
Thermal expansion behavior
Thermal conductivity
Multiphase design residual stress

ABSTRACT

Developing metal matrix composites with low thermal expansion yet high thermal conductivity (λ) has been an ongoing effort in electronic packaging materials due to the growing demand for high-power applications. However, progress has been hindered by the insufficient thermal expansion suppression of conventional low thermal expansion reinforcements or the low λ of negative thermal expansion reinforcements. In this study, this challenge is overcome *via* a multiphase design strategy using ZrW_2O_8 and SiC to co-reinforce the aluminum matrix composites. This approach simultaneously combines the advantages of the ZrW_2O_8 for controlling the coefficient of thermal expansion (CTE) and SiC for improving λ. A controlled CTE-λ balance ($6.22–9.7 \times 10^{-6}\,K^{-1}$, 63.1–131.1 W/mK) can be obtained by varying the volume ratio of ZrW_2O_8 to SiC. The CTE of this composite is significantly lower than that of the 50 vol% SiC/Al composite, while its CTE is approximately equal to that of the 45 vol% ZrW_2O_8/Al composite but with a twofold increase in λ. The good thermal performance of this composite can be attributed to the strong interfacial interactions of SiC and the tailored variation in CTE. Furthermore, simulation and experimental results revealed that the residual stress can be effectively relieved through this strategy. This work presents a straightforward structural design and an effective pathway to manufacture composites with excellent integrated properties.

© 2026 Published by Elsevier B.V. on behalf of Chinese Chemical Society and Institute of Materia Medica, Chinese Academy of Medical Sciences.

With the rapid growth of electronic technology in the direction of high density, high speed, high power and miniaturization, the heat dissipation of electronic components has become one of the technical bottlenecks in the development of the electronic information industry [1–3]. Metal matrix composites, having a high thermal conductivity (λ) and controlled coefficient of thermal expansion (CTE), perform an important role in electronic devices. Nonetheless, due to the high CTE of the high λ metal matrices such as Al ($23 \times 10^{-6}\,K^{-1}$) and Cu ($16 \times 10^{-6}\,K^{-1}$), it is difficult to obtain composites by using conventional low thermal expansion (LTE) reinforcements (*e.g.*, SiC, AlN) matching the CTE of chip semiconductors (*e.g.*, Si, GaAs) even at high ceramic content [4–7]. Alternatively, negative thermal expansion (NTE) reinforcements (*e.g.*, ZrW_2O_8, $PbTiO_3$) can effectively compensate for the positive thermal expansion of the matrix, thus realizing low or even zero thermal expansion composites [8–15]. Unfortunately, these NTE reinforcements generally have a low λ (<15 W/mK), which results in a dramatic decrease in the λ of composites along with a decrease in their CTE [16–22]. To date, most of the studies have mainly focused on improving the performances of λ and CTE in the composites through regulation of the reinforcement distribution and optimization of the preparation process [16–25]. Although these strategies achieve good λ, it is still a great challenge to simultaneously achieve a high level of λ and maintain a low CTE. Therefore, a new design strategy is urgently needed to develop composites with both low thermal expansion and high thermal conductivity for applications requiring high heat dissipation.

The design of multiphase reinforced composites is an effective way to overcome the property trade-off paradox [26–33]. The synergistic combination of multiphase properties has the potential to

* Corresponding authors.
E-mail addresses: xiuzhuhan@163.com (X. Han), changzhou@ustb.edu.cn (C. Zhou).

https://doi.org/10.1016/j.cclet.2025.111849
1001-8417/© 2026 Published by Elsevier B.V. on behalf of Chinese Chemical Society and Institute of Materia Medica, Chinese Academy of Medical Sciences.

realize composites with excellent integrated properties. For example, due to the unique stress distribution mechanism of different phases, the introduction of high-modulus nanoparticles into NTE/Al composites can significantly reduce residual stress and improve mechanical properties [29]. This means that if the introduced phase has a high λ, the λ of the NTE/Al composite is also expected to be significantly improved. In addition, the strong elastic interaction of high-stiffness phases at the interface has been demonstrated to further decrease the CTE of composites [7,34]. For instance, in the diamond/Al composite, the expansion of the Al matrix is strongly limited by the surrounding ultra-stiff diamond particles, and the composite achieves an ultra-low CTE [34]. Therefore, a multiphase design strategy by simultaneously introducing NTE phase and conventional LTE phase into composites is expected to maintain low thermal expansion while achieving a high thermal conductivity.

Here, we use ZrW_2O_8 and SiC to co-reinforce the aluminum matrix composites to show this multiphase design strategy. The effects of different volume ratios of ZrW_2O_8 to SiC on the phase constitution, residual thermal stress, CTE, λ and compressive properties of the composites are investigated. Meanwhile, the low thermal expansion mechanism of the composite is analyzed in detail based on *in situ* temperature-dependent XRD and finite element method. Among them, an aluminum matrix composite with both low CTE ($7.10 \times 10^{-6}\,K^{-1}$) and high λ (87.2 W/mK) was achieved by a multiphase design of 30 vol% ZrW_2O_8 and 20 vol% SiC. This strategy provides an effective framework for the design of materials with low thermal expansion and high thermal conductivity performances.

Owing to the isotropic NTE effect in a wide temperature region caused by low-energy atomic thermal vibrations, ZrW_2O_8 is selected to regulate the thermal expansion of the composites [35–37]. Meanwhile, SiC with LTE, high modulus, and high λ characteristics was selected to regulate the λ of the composites. In this work, the Al matrix content was fixed at 50 vol% to explore the effect of different volume ratios of ZrW_2O_8 to SiC (50:0, 40:10, 30:20, 20:30, 10:40, 0:50) on the thermal performances of the 50 vol% (ZrW_2O_8+SiC)/AlSi composite. These samples are subsequently denoted as "50ZWO-50AlSi", "40ZWO-10SiC-50AlSi", "30ZWO-20SiC-50AlSi", "20ZWO-30SiC-50AlSi", "10ZWO-40SiC-50AlSi", and "50SiC-50AlSi" composites, respectively. Meanwhile, a series of SiC/Al composites and ZrW_2O_8/Al composites were also fabricated in the same process for comparing the thermal properties with the multiphase composites. The XRD patterns of the composites show that the diffraction peak intensity of SiC gradually increases with the rise in SiC content, while that of ZrW_2O_8 gradually decreases (Fig. 1a). In addition, the absence of detectable peaks for the other phases indicates the well-controlled interface structure. This is due to the low temperature rapid sintering process, which avoids damage to the structure of ZrW_2O_8 [16,18,38].

The ZrW_2O_8 generally shows two structures, the low-temperature phase α-ZrW_2O_8 ($\alpha_l = -8.9 \times 10^{-6}\,K^{-1}$, ~448 K, $P2_13$) and the high-temperature phase β-ZrW_2O_8 ($\alpha_l = -4.9 \times 10^{-6}\,K^{-1}$, >448 K, *Pa*-3) [35,36]. The raw ZrW_2O_8 powders are composed of a single α-ZrW_2O_8 (Fig. 1b). However, the diffraction peaks of ZrW_2O_8 are split notably in the composites and the diffraction peaks of the γ-ZrW_2O_8 are observed. The γ-ZrW_2O_8 ($\alpha_l = 1.0 \times 10^{-6}\,K^{-1}$, $P2_12_12_1$) is formed from α-ZrW_2O_8 under pressure of more than 200 MPa [8]. And the existence of γ-ZrW_2O_8 not only weakens the NTE effect of ZrW_2O_8, but also causes a drastic fluctuation in the thermal expansion curve of the composite [37,38]. Interestingly, the relative diffraction intensity of γ-ZrW_2O_8 decreases after the introduction of SiC. The weight fraction of the γ-phase can be determined from Fig. 1b by $f_\gamma = 1 - W_{(\gamma)}/W_{(ZWO)}$. Here, the $W_{(\gamma)}$ represents the diffraction intensity value of $(210)_\gamma$ and the $W_{(ZWO)}$ represents the intensity value of the sum of $(210)_\gamma$ and $(012)_\alpha$. As shown in Fig. 1c, the content of γ-phase in ZrW_2O_8 gradually decreases with the increase in SiC content. In particular, the relative content of γ-ZrW_2O_8 in the 20ZWO-30SiC-50AlSi composite is less than half of that in the 50ZWO-50AlSi composite. Furthermore, it should be noted that the sintering pressure is only 40 MPa in this work, which is far below the stress threshold for the formation of γ-ZrW_2O_8. Nevertheless, due to the significant CTE difference between the ZrW_2O_8 and the Al matrix, huge thermal mismatch stresses (~1 GPa) are generated during the preparation process [8,29]. As a result, the formation of γ-ZrW_2O_8 is caused by thermal mismatch stress. The lower content of γ-ZrW_2O_8 indicates that the residual stresses generated in the composites during the preparation process are relatively low. More details will be discussed in the following section.

To explore the morphology and phase distribution of the multiphase composites, scanning electron microscope measurement was carried out. Due to the similarity of these composites, the microstructure of the 20ZWO-30SiC-50AlSi composite was only studied in detail (Fig. 1d). The particle sizes of ZrW_2O_8 (52.47 μm) and SiC (35.75 μm) show a uniform distribution (Fig. S1 in Supporting information). Moreover, a good spacing (63.65 μm) between particles was maintained. This suggests that the particles are homogeneously distributed in the aluminum matrix. To gain a deeper insight into the interface, a detailed transmission electron microscopy (TEM) characterization was carried out. A smooth and continuous interface in the ceramic/matrix is present in the bright-field TEM image of the SiC/Al interface (Fig. 1e). The enrichment of the elements was not found at the interface (Fig. S2 in Supporting information). Furthermore, a clear interface without microcracks, impurities, and porosity is observed in a high-resolution TEM (HR-TEM) image, suggesting that a good interfacial bonding is formed. For the ZrW_2O_8/Al interface, a smooth and continuous interface can also be observed in Fig. 1f. Nevertheless, the elements Zr, W, O, and Al exhibit a gradient distribution at the interface, and the thickness of the interfacial atomic diffusion layer was approximately 70 nm (Fig. S2 in Supporting information). Meanwhile, no obvious diffraction fringes were observed at the interface in the HR-TEM image and an amorphous interface formed, which may stem from the TEM sample preparation [18]. The good interfacial bonding between the Al matrix and the reinforcement not only reduces interfacial scattering, but also enhances the advantages of the reinforcements for achieving a good CTE-λ balance.

Known as an optimal NTE material, ZrW_2O_8 exhibits its strengths in regulating thermal expansion over a wide temperature region. As shown in Fig. 2a, the sintered 50ZWO-50AlSi composite exhibits uniform low expansion behavior below 400 K and above 420 K. Unfortunately, a dramatic fluctuation from 400 K to 420 K can be found in the thermal expansion curve. Interestingly, this dramatic fluctuation gradually decreases with the rise in SiC content. Furthermore, a stable and smooth thermal expansion behavior can be obtained with a SiC content of up to 30 vol%. To further investigate the effect of SiC content on the CTE of the composites, a heat treatment of 473 K for 6 h was performed to eliminate the γ-ZrW_2O_8 [39,40]. As shown in Fig. 2b, all composites display stable and smooth thermal expansion curves after annealing. Among these, the 20ZWO-30SiC-50AlSi and 10ZWO-40SiC-50AlSi composites exhibit a similar thermal expansion behavior before and after annealing. Therefore, the abnormal expansion in γ-ZrW_2O_8 can be limited by this multiphase design strategy, which is meaningful for the design and preparation of pressure-induced phase transition materials.

Due to the main suppression of the thermal expansion for the aluminum matrix originating from ZrW_2O_8, the introduction of SiC leads to an increase in the CTE (175–325 K) of the composites, as shown in Fig. 2c. Furthermore, a noticeable decrease in CTE can

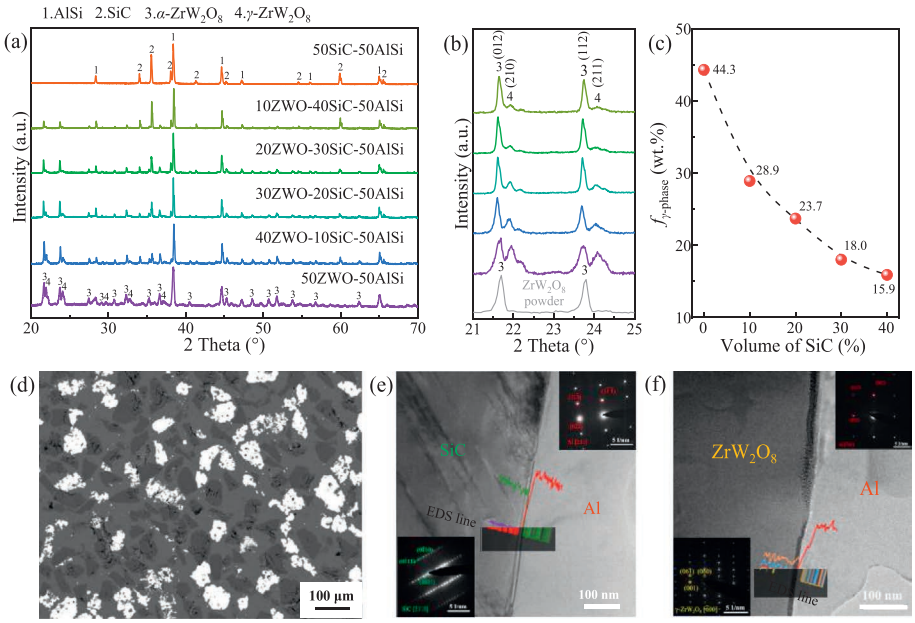


Fig. 1. (a) Room-temperature XRD patterns of the (ZrW_2O_8+SiC)/AlSi composites. (b) Enlargement of the XRD pattern in ZrW_2O_8 from 21° to 25°. (c) γ-Phase content in ZrW_2O_8. (d) SEM image of the 20ZWO-30SiC-50AlSi composite. Bright-field TEM image of the region near the interface of (e) SiC/Al and (f) ZrW_2O_8/Al.

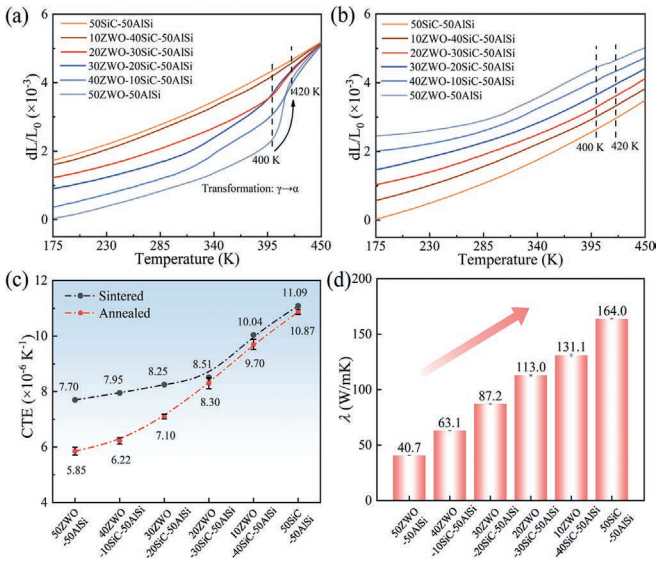


Fig. 2. The linear thermal expansion of the (a) sintered and (b) annealed (ZrW_2O_8+SiC)/AlSi composites. (c) Comparison of CTE for composites before and after heat treatment. (d) The λ of composites.

be observed after annealing, which results from a decrease in the content of γ-ZrW_2O_8 (Fig. 1c). Meanwhile, the CTE of composites cannot be significantly affected by the γ-ZrW_2O_8 phase transformation when the SiC content reaches 30 vol%. Notably, the CTE of the annealed composites shows a progressive upward movement with the rise in SiC content. This unique CTE-increasing trend of the multiphase composites was quite different from previous reports, which may stem from the strong elastic interaction of high-modulus SiC [1,8,12,13,18,20,21]. A detailed discussion is presented in the subsequent sections.

Thermal conductivity is recognized as a measure of the capacity for thermal diffusion, and it carries equal significance to thermal expansion. Due to the aluminum content being limited to 50 vol%, the content of SiC is the key to regulating the λ of the composites. As shown in Fig. 2d, the 50ZWO-50AlSi composite has attractive LTE properties (5.85×10^{-6} K^{-1}), but the low λ (0.51 W/mK) of ZrW_2O_8 causes a dramatic deterioration in its λ (40.7 W/mK) [22,41]. This significantly limits its application requiring high heat dissipation. Interestingly, the λ of the composites increases linearly with the rise in SiC content. Furthermore, this composite also has a good compressive property due to the good interfacial bonding (Fig. S3 in Supporting information). The CTE and λ in the multiphase composites with LTE aluminum matrix composites are compared to show a unique advantage in this strategy [17–19,42–44]. It can be further seen from Fig. S4 (Supporting information) that the CTE of 30ZWO-20SiC-50AlSi composite is similar to that of 45 vol% ZrW_2O_8/Al composite (6.94×10^{-6} K^{-1}), but the λ of the latter (47.3 W/mK) is only half of the former. Meanwhile, the CTE of this composite is far from that of the 50SiC-50AlSi composite (10.87×10^{-6} K^{-1}). And the thermal performance of other ZWO-SiC-AlSi composites also presents a good advantage compared to SiC/Al or ZrW_2O_8/Al composites. Thus, the good CTE-λ balance in the (ZrW_2O_8+SiC)/AlSi composites well demonstrates the feasibility and effectiveness of the multiphase design strategy in the field of electronic packaging materials.

To reveal the regulation of SiC on the thermal expansion of the composites, numerical simulations and experiments were performed to investigate the residual stresses in the composites. The 50ZWO-50AlSi and 20ZWO-30SiC-50AlSi composites (as-sintered) were selected to study the effect of SiC introduction on the stress dispersion mechanism. The residual stresses were analyzed using a micro-zone X-ray residual stress measurement system. When there are residual stresses in the test, the crystal plane spacing is changed and the diffraction angle 2θ varies with the crystal plane azimuth angle (ψ). The (510) plane of ZrW_2O_8 at 118.7° was selected for strain analysis due to its higher diffraction angle and high multiplicity. As shown in Fig. 3a, the diffraction peak shifts to the higher angle with the increase of the ψ value in the 50ZWO-50AlSi composite. This suggests a decrease in crystal plane distance d(510) and the formation of compressive strain in the composite. Intriguingly, the shift of diffraction peak can hardly be observed in the 20ZWO-30SiC-50AlSi composite (Fig. 3b), suggesting the lower residual thermal stress.

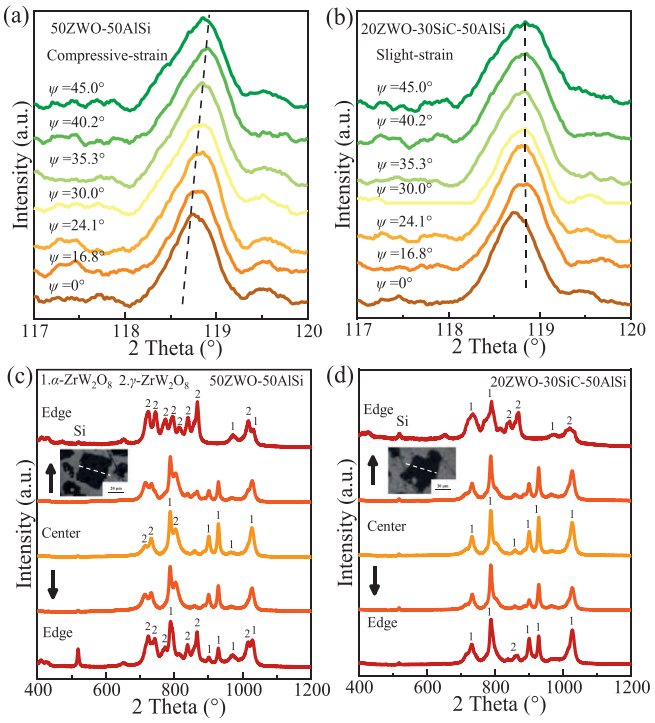


Fig. 3. XRD patterns with ψ values of ZrW_2O_8 in the (a) 50ZWO-50AlSi and (b) 20ZWO-30SiC-50AlSi composites. Raman spectra of (c) 50ZWO-50AlSi and (d) 20ZWO-30SiC-50AlSi composites.

Raman was sensitive to the local atomic environment and transition, which was another way to characterize the thermal residual stress and γ-ZrW_2O_8 content in the ZrW_2O_8/Al composites [45–49]. The line scanning Raman spectra at room temperature of ZrW_2O_8 particles in the composites are depicted in Figs. 3c and d. In the 50ZWO-50AlSi composite (Fig. 3c), the modes of α-phase and γ-phase can be observed in the center of the particle [8]. Additionally, the intensity of α-phase decreases while that of γ-phase gradually enhances as the distance increases (compositionally from the center to the edge in the particle), suggesting the formation of compositional gradients in this particle. In particular, the edges of the particles show nearly complete Raman peaks of the γ-phase. Interestingly, a similar trend but a relatively lower intensity for γ-phase modes at the particle edge can be observed in the 20ZWO-30SiC-50AlSi composite (Fig. 3d). This indicates that the residual stresses are not enough to induce significant γ-ZrW_2O_8 formation, which is in good agreement with the content of γ-ZrW_2O_8 measured by XRD (Fig. 1c).

The residual stress was also calculated by numerical simulation in the 50ZWO-50AlSi and 20ZWO-30SiC-50AlSi composites, as shown in Fig. S5 (Supporting information). In the 50ZWO-50AlSi composite, the giant stress (400 MPa) concentration appears at the edge of ZrW_2O_8 particle, which is consistent with the previous study [8]. Interestingly, the residual stress in the 20ZWO-30SiC-50AlSi composite reduces to 200 MPa. This can be attributed to the fact that the difference in CTE between SiC and the aluminum matrix is only half of that between ZrW_2O_8 and the aluminum matrix. Furthermore, the stress concentration on the SiC surface (300 MPa) is very significant, which is higher than that of ZrW_2O_8 (200 MPa). This is mainly due to the high modulus characteristics of SiC that make it bear more residual stresses during the preparation. Thus, the above numerical simulation and experiments show that the SiC not only reduces the CTE difference between ZrW_2O_8 and the Al matrix, but also bears more residual stress. The synergistic effect of these two factors reduces the residual stress acting on ZrW_2O_8, thus decreasing the formation of γ-ZrW_2O_8.

To reveal the LTE mechanism of (ZrW_2O_8+SiC)/AlSi composites, the structural evolution of the sintered 40ZWO-10SiC-50AlSi composite (as-sintered) during heating was systematically studied by means of *in situ* temperature-dependent XRD (Fig. 4a and Fig. S6 in Supporting information) [50]. As shown in Fig. 4a, the diffraction peaks of ZrW_2O_8 show significant shifts and variations during heating. From the partial enlargement in Fig. 4b, the XRD spectra of ZrW_2O_8 can be divided into four parts. Firstly, the coexisting α-phase and γ-phase can be observed at 173 K. And the diffraction peaks of α-phase gradually shift to higher angles from 173 K to 413 K, suggesting that the volume shrinkage accompanied by the low-energy atomic thermal vibrations occurs. From 413 K to 433 K, the diffraction peak intensity of γ-phase gradually decreases. Moreover, the diffraction peaks of γ-phase are hardly observed at 433 K, suggesting that the $\gamma \rightarrow \alpha$ phase transition has occurred. From 433 K to 453 K, the diffraction peak intensity of α-phase gradually decreases, while that of β-phase gradually increases. Besides, the diffraction peaks of α-phase can hardly be observed at 453 K, indicating that the $\alpha \rightarrow \beta$ phase transition has occurred. Finally, as the temperature increases from 453 K to 473 K, a single diffraction peak of the β-phase is observed, which gradually shifts to a higher angle. Furthermore, the diffraction peaks of SiC and Al matrix gradually shift to lower angles from 173 K to 473 K, suggesting that a persistent volume expand during heating. Compared with the linear thermal expansion data in Fig. 2a, the change of the diffraction peaks of ZrW_2O_8 is consistent with the change trend of the thermal expansion curves. Therefore, the abnormal expansion of the composites at 400 K results from the phase transition of γ-ZrW_2O_8 to α-ZrW_2O_8. The gradual decrease of this abnormal expansion with the rise in SiC content originates from the decrease in γ-ZrW_2O_8 content.

The intrinsic CTE of each phase was obtained by Rietveld refinements based on the *in situ* temperature-dependent XRD data (Fig. S6 in Supporting information). The results show that the AlSi, SiC, and ZrW_2O_8 from 173 K to 323 K show a CTE of 21.01, 4.50, and $-8.10 \times 10^{-6}\,K^{-1}$, respectively (Fig. 4c). Meanwhile, the CTE of the 40ZWO-10SiC-50AlSi composite is calculated to be $8.81 \times 10^{-6}\,K^{-1}$ by the Rule of Mixture. Thus, the lattice shrinkage of ZrW_2O_8 and the lattice expansion of SiC and AlSi synergistically contribute to the formation of LTE aluminum matrix composites.

The LTE mechanism of the composites was further analyzed by using ROM and Turner models (Fig. 4d). The ROM model assumes that thermal stresses are uniformly distributed in the composite without considering interfacial effects [51]. Thus, the CTE increases linearly in the ROM model with the rise in SiC content. However, the Turner model assumes that thermal strain in the composite is uniform, which requires a consideration of the modulus of each phase [52]. The CTE in the Turner model shows a progressive upward movement, consistent with the trend in this study. This originates from the fact that the modulus of SiC (400 GPa) is substantially higher than that of ZrW_2O_8 (90 GPa) and Al (70 GPa). Meanwhile, this also explains why the calculated intrinsic CTE (Fig. 4c, $8.81 \times 10^{-6}\,K^{-1}$) is higher than the experimental value (Fig. 2c, $6.22 \times 10^{-6}\,K^{-1}$) for the 40ZWO-10SiC-50AlSi composite. Notably, the stronger interfacial interactions inhibited the increase of CTE of the composites at lower SiC content. This structural advantage gradually decreases with further increase in SiC content, resulting in insufficient interfacial interactions to suppress the sharp increase in CTE. Therefore, the volume ratio of a small amount of SiC and more ZrW_2O_8 is the promising solution to significantly improve the λ and maintain the low CTE.

In summary, a multiphase design strategy is adopted to achieve both low thermal expansion and high thermal conductivity. This strategy exhibits a unique advantage in terms of thermal expansion

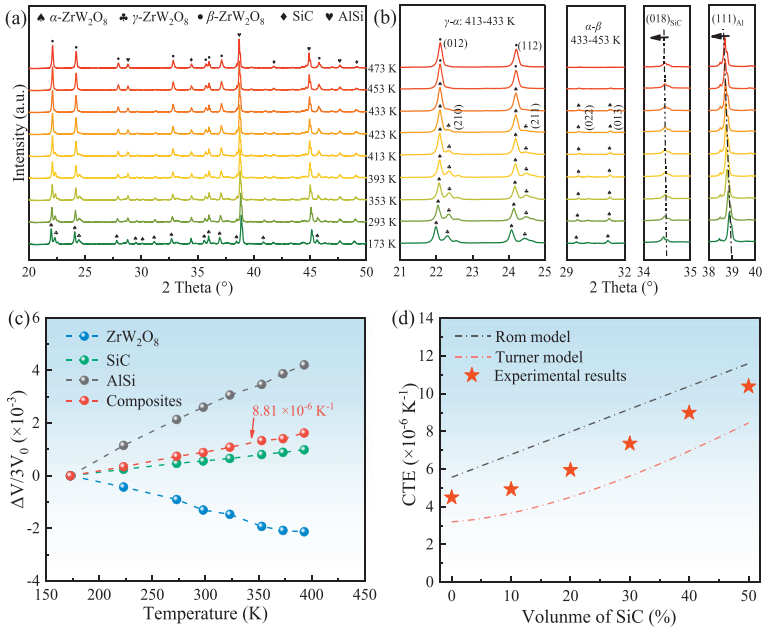


Fig. 4. (a) XRD pattern of the 40ZWO-10SiC-50AlSi composite from 173 K to 473 K. (b) enlargement of the XRD patterns from 21° to 25°, 29° to 32°, 34° to 35°, and 38° to 40°. (c) Relative evolution of lattice parameter. (d) CTE of the (ZrW_2O_8+SiC)/AlSi composites and the theoretical values estimated by the ROM and Turner models.

and thermal conductivity compared to ZrW_2O_8/Al and SiC/Al composites. The low thermal expansion originates not only from the NTE ZrW_2O_8 and LTE SiC, but also from the additional expansion hindrance provided by the stiff SiC within the Al matrix. Meanwhile, the high thermal conductivity of SiC significantly enhances the overall thermal conductivity of the composites. Additionally, finite element simulations and experimental results show that the introduction of SiC reduces the formation of γ-ZrW_2O_8 by mitigating residual stress generation during preparation. This multiphase design strategy and the associated mechanisms that enhance thermal conductivity without significantly increasing the coefficient of thermal expansion are promising for developing metal matrix composites with excellent integrated properties.

Declaration of competing interest

The authors declare that they have no known competing financial interests or personal relationships that could have appeared to influence the work reported in this paper

CRediT authorship contribution statement

Jinrui Qian: Writing – original draft, Investigation, Data curation. **Yue Sun:** Writing – review & editing, Investigation, Data curation. **Feixiang Long:** Writing – review & editing, Data curation. **Yiqing Liu:** Investigation. **Guozhen Chang:** Investigation. **Yuzhu Song:** Visualization, Formal analysis. **Naike Shi:** Visualization, Formal analysis. **Andrea Sanson:** Visualization. **Xiuzhu Han:** Visualization, Formal analysis. **Chang Zhou:** Writing – review & editing, Visualization, Supervision, Investigation, Funding acquisition, Formal analysis, Conceptualization. **Jun Chen:** Supervision, Funding acquisition.

Acknowledgments

This work was supported by the Beijing Outstanding Young Scientist Program (No. JWZQ20240101015), the National Natural Science Foundation of China (No. 22205016), and the National Key Research and Development Program of China (No. 2022YFE0109100). We acknowledge Prof. Xianran Xing for providing laboratory X-ray diffraction at the Institute of Solid State Chemistry, University of Science and Technology Beijing.

Supplementary materials

Supplementary material associated with this article can be found, in the online version, at doi:10.1016/j.cclet.2025.111849.

References

[1] C. Zhou, H. Zhong, H. Lu, et al., Ceram. Int. 49 (2023) 27958–27964.
[2] Y. Song, N. Shi, S. Deng, et al., Prog. Mater Sci. 121 (2021) 100835.
[3] M. Ai, Y. Song, F. Long, et al., Adv. Sci. 11 (2024) 2404838.
[4] T. Huber, H. Degischer, G. Lefranc, T. Schmitt, Compos. Sci. Technol. 66 (2006) 2206–2217.
[5] P. Gudlur, A. Forness, J. Lentz, et al., Mat. Sci. Eng. A: Struct. 531 (2012) 18–27.
[6] S. Roy, K. Scheell, E. Bucharsky, et al., Mat. Sci. Eng. A: Struct. 743 (2019) 339–348.
[7] T. Nam, G. Requena, P. Degischer, Compos. Part A 39 (2008) 856–865.
[8] C. Zhou, Y. Zhou, Q. Zhang, et al., Compos. Part B 211 (2021) 108678.
[9] J. Guo, M. Fang, Q. Liu, et al., Chin. Chem. Lett. 35 (2024) 108957.
[10] C. Zhou, Q. Zhang, S. Liu, et al., Phys. Chem. Chem. Phys. 19 (2017) 11778–11785.
[11] A. Goodwin, M. Calleja, M. Conterio, et al., Science 319 (2008) 794–797.
[12] C. Zhou, Q. Zhang, X. Tan, et al., Material 6 (2019) 100289.
[13] J. Miao, J. Liu, X. Wu, et al., Sci. Eng. Compos. Mater. 25 (2018) 95–100.
[14] H. Cao, Y. Su, D. Zhang, et al., Compos. Part B 223 (2021) 109080.
[15] H. L., C. Zhou, Y. Song, et al., Nat. Commun. 16 (2005) 211.
[16] C. Zhou, C. Liu, Y. Zhou, et al., Ceram. Int. 49 (2023) 34074–34082.
[17] Y. Zhou, C. Zhou, Z. Wang, et al., Ceram. Int. 48 (2022) 25826–25832.
[18] L. Xie, J. Lin, X. Zhong, et al., Ceram. Int. 49 (2023) 35617–35622.
[19] C. Zhou, Z. Tang, X. Kong, et al., Acta Mater 275 (2024) 120076.
[20] Y. Zhou, C. Zhou, Y. Wu, et al., Ceram. Int. 49 (2023) 34472–34480.
[21] Y. Zhou, L. Zhang, J. Qian, et al., Material 16 (2023) 5919.
[22] Y. Qiao, N. Xiao, Y. Song, et al., ACS Appl. Mater. Interfaces 12 (2020) 57228–57234.
[23] C. Kennedy, M. White, Solid State Commun. 134 (2005) 271–276.
[24] B. Dong, C. Wei, J. Lin, et al., J. Mater. Sci. Technol. 213 (2024) 90–97.
[25] B. Dong, X. Guo, P. Tong, et al., J. Alloys Compd. 978 (2024) 173504.
[26] B. Hang, S. Liu, X. Wang, et al., Mat. Sci. Eng. A: Struct. 804 (2021) 140517.
[27] C. Liang, M. Hamidinejad, L. Ma, et al., Carbon 156 (2020) 58–66.
[28] M. Zhou, L. Ren, L. Fan, et al., J. Alloys Compd. 838 (2020) 155274.
[29] C. Zhou, Y. Zhou, S. Liu, et al., J. Alloys Compd. 907 (2022) 164444.
[30] C. Ding, W. Gan, X. Hu, et al., Mat. Sci. Eng. A 797 (2020) 140105.
[31] R. Wang, Y. Tian, X. Gao, L. Jiang, Chin. Chem. Lett. 36 (2025) 110395.
[32] L. Li, P. Ji, M. Huang, et al., Chin. Chem. Lett. 35 (2024) 109144.
[33] T. Long, P. Chen, B. Feng, et al., Chin. Chem. Lett. 35 (2024) 109267.

[34] N. Li, Y. Zhang, Y. Zhang, et al., Mater. Today Phys. 28 (2022) 100901.
[35] T. Mary, J. Evans, T. Vogt, Science 272 (1996) 90–92.
[36] Y. Sato, Y. Yamamura, K. Saito, Y. Ikuhara, J. Am. Chem. Soc. 134 (2012) 13942–13945.
[37] N. Shi, L. Fan, Y. Xu, et al., Small 20 (2024) 2312289.
[38] H. Holzer, D. Dunand, J. Mater. Res. 14 (1999) 780–789.
[39] G. Wu, C. Zhou, Q. Zhang, et al., Scripta Mater. 96 (2015) 29–32.
[40] C. Zhou, Q. Zhang, M. Zhang, G. Wu, J. Alloys Compd. 718 (2017) 356–360.
[41] A. Ramirez, G. Kowach, Phys. Rev. Lett. 80 (1998) 4903–4906.
[42] J. Sethi, S. Das, K. Das, J. Alloys Compd. 774 (2019) 845–855.
[43] D. Jacobson, A. Ogilvy, Materwiss Werksttech 34 (2003) 381–384.
[44] F. Stadler, H. Antrekowitsch, W. Fragner, et al., Mat. Sci. Eng. A 560 (2013) 481–491.
[45] X. Zhang, Y. Liu, N. Wang, et al., Microstructures 4 (2024) 2024002.
[46] Y. Fang, S. Deng, T. Li, Chin. Chem. Lett. 34 (2023) 107796.
[47] L. Wang, S. Zhan, Y. Ruan, et al., J. Rare Earths 42 (2024) 2285–2292.
[48] Y. Yang, Z. Lin, R. Li, et al., Microstructures 1 (2021) 2021002.
[49] X. Pan, Y. Cui, Z. Wang, Chin. Chem. Lett. 35 (2024) 109567.
[50] Y. Li, S. Chou, Y. Xiao, Chin. Chem. Lett. 36 (2025) 110389.
[51] Z. Karadeniz, D. Kumlutas, Compos. Struct. 78 (2007) 1–10.
[52] P. Turner, J. Res. Nat. Bur. Stand. 37 (1946) 239.